Journal of Turbulence
Volume 7, No. 22, 2006

Taylor & Francis
Taylor & Francis Group

Numerical studies of turbulent particle fluxes into perfectly absorbing spherical surfaces

G. BOFFETTA†, H. L. PÉCSELI*,‡ and J. TRULSEN††

†Dipartimento di Fisica Generale, via Pietro Giuria 1, I-10125 Torino, Italy
‡University of Oslo, Institute of Physics, Box 1048 Blindern, N-0316 Oslo, Norway
††University of Oslo, Institute of Theoretical Astrophysics, Box 1029 Blindern, N-0315 Oslo, Norway

With reference to studies of the influence of turbulence on the feeding process of aquatic micro-organisms, we analyze particle fluxes into absorbing surfaces in turbulent flows by numerical simulations. The simultaneous trajectories of many point particles are followed in time in a fully three-dimensional solution of the turbulent flow described by the Navier–Stokes equation. Selecting one of these points to represent a predator, while the others are considered as prey, we obtain estimates for the time variation of the statistical average of particle fluxes into a co-moving "sphere of interception". The essential restriction in the model, when applied to aquatic micro-organisms, is that self-induced motions are ignored. Particles are assumed to be absorbed when crossing the surface. In this sense, the problem can be analyzed as the one involving a perfectly absorbing surface. The variation of the particle flux with the radius in the absorbing sphere, as well as the variation with basic flow parameters is well described by a simple scaling law, expressed in terms of the radius of the sphere and the energy dissipated per mass unit. The results also agree well with experimental results. In the present study, we obtain a unique signal-to-noise ratio in the estimates. The analysis is extended by inclusion of another dataset, with a somewhat smaller Reynolds number. The scaling laws obtained by a simple dimensional reasoning agree well for the two datasets. The numerical simulations refer to two different Reynolds numbers, but the scaling laws verified for these conditions can then be applied generally for other flows, provided the basic assumptions are fulfilled: the turbulence has to be fully developed so that a universal subrange exists, and the spatial scales defined by the radii of the absorbing spherical surfaces have to be restricted to this subrange.

1. Introduction

Often the problem of turbulent diffusion in neutral turbulent flows is analyzed as an initial value problem [1–3]. However, for many applications, a boundary value problem is more relevant. Here, we consider a problem which has received particular interest by its importance for aquatic micro-organisms. For small predators, fish larvae or copepods, for instance [4], it is often assumed that their self-induced motion is small or negligible, and that they are passively convected by the local flow velocity, at least to a good approximation. Similarly, it can be assumed that their food, or "prey", (micro-zooplankton, for instance) is also passively convected by the same flow. The feeding process can be modeled by assuming that any individual prey entering a suitably defined "sphere of interception" is captured with certainty. In turbulent waters, the predator–prey encounter rate is thus related to the problem of relative diffusion, but now considered as a boundary value problem, with the condition that the prey

*Corresponding author. E-mail: hans.pecseli@fys.uio.no

Journal of Turbulence
ISSN: 1468-5248 (online only)
http://www.tandf.co.uk/journals
DOI: 10.1080/14685240600573138

Table 1. Simulation I lasts 1167 time steps with $dt = 0.005$, and simulation II lasts 1841 time steps with $dt = 0.0023$.

dx	$2\pi/512 = 0.012\,272$	$2\pi/1024 = 0.006\,1359$
ν	2.05×10^{-3}	8.8×10^{-4}
ϵ	$0.885\,3212$	$0.810\,878$
$E = \frac{1}{2}\langle u^2 \rangle = \frac{3}{2}\langle u_{\rm rms}^2 \rangle$	3.01	2.96
$u_{\rm rms}$	1.42	1.40
λ	0.2642	0.179
Re_λ	183	286
η	$0.009\,93 = 0.81\ dx$	$0.0054 = 0.88\ dx$
τ_η	0.048	0.033
T	5.84	4.23

concentration vanishes at the surface of the sphere of interception. This sphere is moving with the flow so that it has at all times the same particle at its center. This is the standard model for this particular problem [5–7]. The surface is thus "virtual" in the sense that it does not disturb the flow. The general interest in this particular problem arises essentially from the simple observation that the food concentration in the near region of a predator will rapidly be depleted, and without any self-induced motion a predator will be starving, unless the prey in the vicinity of its sphere of interception is continuously replaced by turbulent motions in the flow.

The problem of predator–prey encounter rates has been studied in controlled laboratory experiments [8], and also by numerical simulations [9]. We here present a study based on two datasets (sets I and II) from numerical solutions of the Navier–Stokes equation in three spatial dimensions, performed in a $512 \times 512 \times 512$ and a $1024 \times 1024 \times 1024$ system of grid-points for extended time periods of 1167 and 1841 time steps, respectively [10]. The system is periodic in all three directions. From the numerically obtained flow field, a large number ($\sim 10^5$) of point particle trajectories are constructed. The basic data for the simulations are given in table 1, where Re_λ denotes the Reynolds number and the Kolmogorov micro-scale is η, the notation for the parameters being standard [10]. For both simulations, we have ϵ to be approximately the same, but the two Reynolds numbers as well as the two Kolmogorov scales are substantially different. The universal subranges for the two cases will consequently be different. The dataset with the largest Reynolds number, see table 1, is our reference.

One important new result of the present analysis is a demonstration of a scaling law for the turbulent particle flux; in terms of the radius $\mathcal{R}$ in the sphere of interception. An empirical function is obtained for the entire time variation of the average flux, in particular also its asymptotic value is obtained with high accuracy. This asymptotic value is the most interesting one for the biological applications. The scaling law is found to be valid for scales where also the universal Kolmogorov–Oubokhov law applies for the second-order velocity structure function.

The simulations analyzed here can, by proper scaling of the variables, be directly applied as models for turbulent flows with the Reynolds numbers listed in table 1. The numerical analysis uses dimensionless numbers, which have to be related to physical quantities for practical applications. We take the numerical value from the simulations to represent a physically realistic quantity, which can have different values for varying conditions. Thus we have [6, 11], typical parameters as those summarized in table 2. The Kolmogorov scales given in computational units in table 1 should be scaled to physical units as given in, for instance, table 2. These length scales should in turn be compared to millimeter-scale capture ranges of predators in nature. For herring larvae an estimated contact radius is $\sim$3 mm, for instance [12, 13], for other species it can be smaller.

Table 2. The Kolmogorov length scale is here η and the specific energy dissipation (dissipated energy per gram fluid) is ϵ. The Kolmogorov times scale is denoted by τ_η.

Open ocean	$\epsilon \sim 10^{-4} - 1$ mm^2 s^{-2}	$\eta \sim 10 - 1$ mm	$\tau_\eta \sim 95 - 0.95$ s
Shelf	$\epsilon \sim 10^{-1} - 1$ mm^2 s^{-2}	$\eta \sim 2 - 1$ mm	$\tau_\eta \sim 3.0 - 0.95$ s
Coastal zone	$\epsilon \sim 10^{-1} - 10^2$ mm^2 s^{-2}	$\eta \sim 2 - 0.2$ mm	$\tau_\eta \sim 3.0 - 0.095$ s
Tidal front	$\epsilon \sim 10$ mm^2 s^{-2}	$\eta \sim 0.5$ mm	$\tau_\eta \sim 0.3$ s

For comparison with naturally occurring turbulence, we can, for instance, select a value for η and determine a scaling factor making it consistent with that of the simulations. With $\nu \approx 0.88 \times 10^{-6}$ m^2 s^{-1} for water we have a scaling factor of 10^3 for viscosity in the reference simulation. By this we determine the scaling factor for $\epsilon = \nu^3/\eta^4$, as well as for the Kolmogorov time scale $\tau_\eta = (\nu/\epsilon)^{1/2}$, consistent with table 2. The dimensionless simulation Reynolds number will be a characteristic of the fluid as well, and with η given, this determines the "outer" scale $\mathcal{L}$. Hereby a relation is established between the simulation and the physical spatial scales, noting that the Kolmogorov times scale τ_η is not an independent parameter. The relation between the numerical and physical mean square fluctuation levels $\langle u^2 \rangle^{1/2}$ is established by $\langle u^2 \rangle \sim (\epsilon \mathcal{L})^{2/3}$, where again $\mathcal{L}$ is the scale size of the largest energy containing eddies in the system [14]. It is important to emphasize that the scaling laws verified for the present parameters can with confidence be applied outside the parameter ranges analyzed here. As long as the relevant length scale of the sphere of interception is within the universal subrange, the scaling laws discussed in the present paper are supposed to be valid, provided of course that the turbulence is fully developed so that a universal subrange exists.

2. Data analysis

With the records of many simultaneous trajectories being available, we can now select one of these to represent the predator, while labeling all the others as prey. In figure 1, we show a sample trajectory, prepared for three-dimensional visualization [15]. We can select a

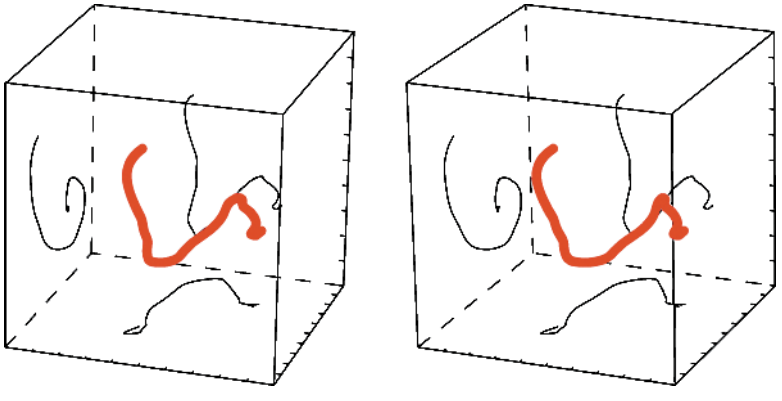

Figure 1. Sample trajectory obtained from the simulations. The figure allows a stereoscopic, three-dimensional view, by focusing the eyes approximately 20 cm behind the plane of the paper or computer screen. (It requires a little exercise. In our experience, the distance to the eyes is not so critical provided it is sufficiently large, but it is essential that the figure is kept plane and horizontally aligned with the observer's eyes.) A similar type of presentation of curves in 3 dimensions was used in several presentations, for instance [15], where many examples are found. The thick red curve is the trajectory, the black curves are projections at the back, bottom, and left sides of the box, respectively. The side-length of the box is 2π.

predetermined radius $\mathcal{R}$ of a sphere of interception, and remove all the points which happen to be inside this sphere at the initial time. During the subsequent Lagrangian motion of the reference "predator", we count the number of prey entering its co-moving sphere of interception between successive time steps. Each time a point enters, it is "eaten" in the sense that it is removed from the data base. Here we are only interested in the time evolution of the prey flux for times up to an eddy turn-over time, $\tau_F \equiv \mathcal{L}/\langle u^2 \rangle^{1/2}$, which is within the time-span of the simulations. As long as $\mathcal{R}$ is much smaller than the size of the measuring volume (here 2π), we can with negligible error assume the prey concentration to be constant at large distances, corresponding to ideally infinite systems. By choosing a large number of realizations, we can give an estimate for the ensemble-averaged Lagrangian prey flux after time of release. Parts of the analysis here follow the procedure used for analyzing data from a laboratory experiment [16]. With the present large database, we are able to present results with a hitherto unprecedented accuracy. It should be noted that these numerical simulations have a Reynolds number approximately three times that of the laboratory experiment [17]. Also, we emphasize that there is one basic difference between a laboratory experiment and the present numerical analysis: here the turbulence is driven uniformly over space [10], while in a laboratory experiment, where the turbulence is generated by moving grids, we have basically *decaying turbulence*, in the sense that the energy in volume element of the fluid decays, on average, as it is followed in the region between the two grids [17, 18].

In figure 2, we show examples for the time varying flux to a self-consistently moving sphere of interception with a given radius, $\mathcal{R}$, for our reference dataset. This flux is the result of a competition between, on one hand, the depletion of trajectories labeled "prey" in the vicinity of the reference point, and on the other hand the influx of such point particles due to the turbulent motions in the flow. In each realization, we divide the flux by the initial prey density for that particular realization, and the result thus represents the prey-flux for unit density. For small values of the radius, $\mathcal{R} \ll L \equiv 2\pi$, we find that the flux level is almost constant in time. A trend for an initial decrease becomes conspicuous as the radius is increased. We note that figure 2 is deceiving in one respect by indicating that the fluctuation level decreases for small radii. In reality the *relative* noise level is increasing for decreasing

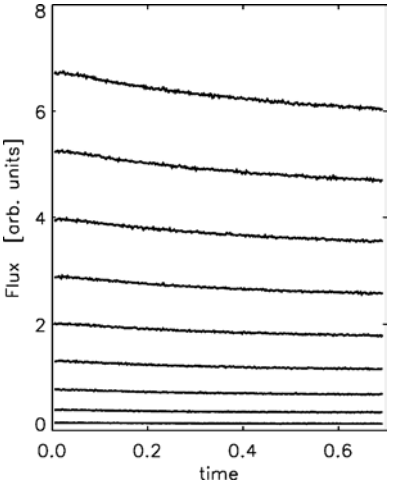

Figure 2. Time variation of the estimate for the ensemble averaged particle flux for unit density $\langle J(t) \rangle / n_0$, to spheres with different radii, $\mathcal{R} = 0.3$–1.0, in steps of 0.1. The selected radii are all within the universal subrange. For this case, we have $Re_\lambda = 286$.

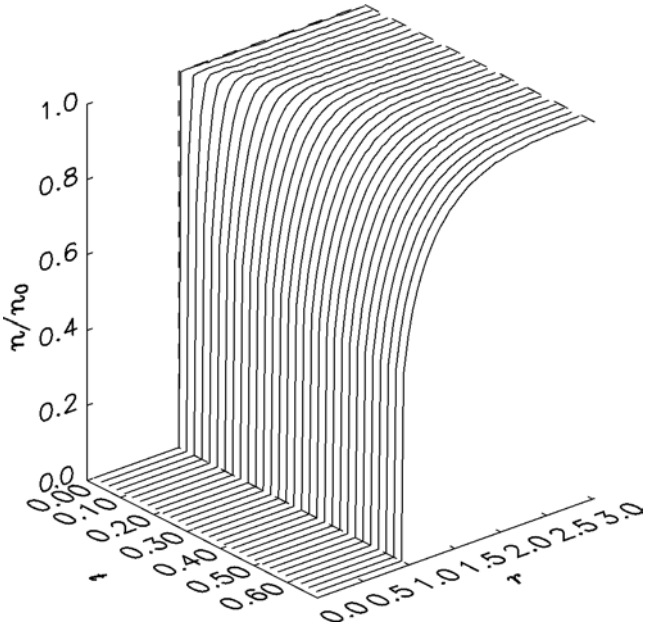

Figure 3. Space-time evolution of the normalized average density around an absorbing spherical surface moving with the flow, for $\mathcal{R} = 1$. Note the steep concentration gradients at the surface $r = \mathcal{R} = 1$.

$\mathcal{R}$, since only a relatively small number of particles contributing to the fluxes for small spheres.

To illustrate the space-time variation of the average particle density in the flow surrounding the selected reference test particle, we show in figure 3 the radial variation of the particle concentration for several times. The problem is spherically symmetric, so the radial variable suffices. Initially, we have by construction zero concentration inside the reference sphere (here chosen to have unit radius). *Outside* the sphere we have a uniform concentration of prey at $t = 0$. At later times, the prey concentration is depleted in the near vicinity of the reference sphere due to the absorption at the surface, while we at the same time have an influx of prey from the unperturbed particle concentration at large r. We note the high numerical accuracy in the result. The turbulence is time stationary in a statistical sense, but the turbulent particle flux is not a time stationary random process (evidently) since the particle population is slowly depleted. The average asymptotic steady-state particle distribution is a result of a statistical equilibrium between absorption at the spherical surface and the new particles being mixed in from large distances. It is interesting to note the steep gradient at the surface of the reference sphere, here $\mathcal{R} = 1$. If the fluxes were to be modeled by a diffusion equation, the diffusion flux determined as the product of a diffusion coefficient and the concentration gradient at $r = \mathcal{R}$, would give very large fluxes, in variance with the observations. We tend to conclude that such a diffusion model can only serve as an illustration.

3. Model discussion

The simplest approach to an analytical expression for the particle flux to a perfectly absorbing surface can be obtained by dimensional reasoning. For scale sizes $\mathcal{R}$ in the universal subrange of the turbulence, where viscosity is immaterial, we have only one length scale, namely $\mathcal{R}$

and one time scale, $\mathcal{R}^{2/3}/\epsilon^{1/3}$. A density dependence of the particle flux is trivial: doubling the particle density uniformly over the system implies a doubling of the flux. Hence we are only interested in the average particle flux divided by the reference particle density, taken at infinity, $\langle J\rangle/n_0$. The only possible dimensionally correct combination is then

$$\frac{\langle J\rangle}{n_0} = \mathcal{R}^{7/3}\epsilon^{1/3} F\left(\frac{t\epsilon^{1/3}}{\mathcal{R}^{2/3}}\right), \tag{1}$$

where F is a dimensionless function of a dimensionless temporal variable. This function is unknown, but from basic physical arguments, we can expect it to have a finite asymptotic numerical value for $t \to \infty$, this value being assumed to be universal. One important result of our analysis is an empirical estimation of the universal function F in (1) and in particular its asymptotic value for large normalized times.

Alternatively, dynamic model equations can be found for the problem. The prey flux to a sphere of interception moving self-consistently with the flow has been modeled by, for instance, a simple diffusion equation. With a properly chosen diffusion coefficient, which depends on spatial separations, but independent of time [7], the prey flux can be evaluated. The diffusion coefficient is found as the product of a velocity $\sim (\epsilon r)^{1/3}$, characterizing the scale determined by r, and the length-scale which is also the separation coordinate r. For predator–prey separations within the universal range of the Kolmogorov–Oubokhov structure function, the equation proposed is actually identical to the one suggested by Richardson in his study of distance-neighbor functions [1]

$$\frac{\partial}{\partial t} n(r,t) = C\frac{\epsilon^{1/3}}{r^2}\frac{\partial}{\partial r} r^{10/3}\frac{\partial}{\partial r} n(r,t)\,, \tag{2}$$

written for spherically symmetric geometry, with r being the radial coordinate taken from the position of the predator, and C being a constant, related to the Richardson constant C_R. To illustrate this relation we use Richardson's *distance-neighbor function*, which states that the probability of finding two particles in a small volume $\mathrm{d}^3\mathbf{r}$ around a position $\mathbf{r}$ at at time t is $P(\mathbf{r},t)\mathrm{d}^3\mathbf{r}$, given that they initially, at $t = 0$, were infinitesimally close. The Richardson law in spherical symmetry then states that

$$\langle r^2\rangle \equiv \int_0^\infty r^2 P(r,t) 4\pi r^2 \mathrm{d}r = C_R \epsilon t^3\,. \tag{3}$$

The relation (3) serves to define the Richardson constant, where we are aware that also other definitions can be found [19]. The definition (3) was used for comparison with recent experimental as well as numerical results [17, 20]. Note that the Richardson law can be obtained from several model equations [2, 17]. Experiments [17] as well as numerical studies [20] indicate that $C_R \approx 0.5$, although the uncertainty on this estimate is negligible.

With the function P satisfying (2) we have the normalized expression

$$P(r,t) = \frac{9}{70\pi^{3/2}}\sqrt{\frac{3}{2}}\left(\frac{3}{2C\epsilon^{1/3}t}\right)^{9/2}\exp\left(-\frac{9r^{2/3}}{4C\epsilon^{1/3}t}\right), \tag{4}$$

which finally gives $C = (3/2)(3C_R/143)^{1/3}$.

From (2), it is easy to derive a steady-state diffusion flux to a sphere with radius $\mathcal{R}$, as the surface area $4\pi\mathcal{R}^2$ multiplied by the product of the diffusion coefficient obtained for $r = \mathcal{R}$ and the gradient of the density, also at $r = \mathcal{R}$ [16]. In particular, we find the asymptotic result consistent also with the previous results [7]

$$\frac{J_\infty}{n_0} = \frac{28\pi}{3} C\epsilon^{1/3}\mathcal{R}^{7/3}, \tag{5}$$

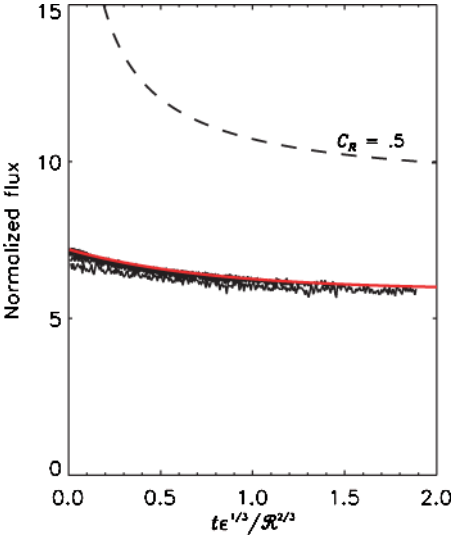

Figure 4. Normalized presentation of the data in figure 2, here for $\mathcal{R} \geq 0.2$ in steps of 0.1. The dashed line represents result for the flux function obtained by solving (2). The red line gives the empirical relation (6). The longest curves (in time) correspond to the smallest $\mathcal{R}$.

where n_0 is the constant prey density at $r \to \infty$. In figure 4, we show (with a dashed line) a numerical solution of the time varying flux, by use of a normalized density obtained from (2).

A recent study of particle pair releases in turbulent flows in a controlled laboratory experiment [17] has given support for the applicability of the model equation (2), at least for the times and spatial separations investigated there. For conditions with scales larger than the integral length scale [21], it was on the other hand found that a diffusion equation with a simple diffusion coefficient as suggested by Batchelor [2] was appropriate. These two cases [17, 21] referred to particle releases considered as initial value problems. A description based on a diffusion equation can be applied for analyzing relative diffusion, but it is also well known that one cannot expect that a diffusion coefficient depending solely on relative times or spatial separations will be universally applicable for this problem [3].

4. Discussions

In order to compare our analysis with analytical results, we re-plot the data from figure 2 in a normalized form i, see figure 4. It turns out to be an advantage to consider two separate intervals for $\mathcal{R}$. As long as $\mathcal{R} > 0.2$ in the present computational units, as in figure 4, we find an excellent agreement with the scaling obtained by the dimensional analysis. We have thus presented an empirical result for the function F in (1), with high accuracy. Its asymptotic constant value is found to be 5.9, with an accuracy of $\pm 3\%$. Empirically, we find that the expression

$$F = 5.9 + 1.3 \exp(-1.3 t\epsilon^{1/3}/\mathcal{R}^{2/3}), \tag{6}$$

gives an excellent approximation to the normalized flux in figure 4. Note that while the curves in figure 2 all have the same temporal duration, their lengths become different when presented in normalized time units. Also, we mention that the relative noise level, for a given number of predator realizations is largest for the smallest radii, since there are fewer particles contributing

to the flux for small separations. To partly compensate for this effect, we have chosen a larger number of realizations in our analysis for the smaller $\mathcal{R}$-values. Some of the implications of (6) are discussed in Appendix A. When applied to a practical problem, we are usually interested in the asymptotic flux only. In that case we can use $J_\infty \approx 5.9\, n_0\, \epsilon^{1/3} \mathcal{R}^{7/3}$, with the relevant flow parameters inserted, see for instance table 2.

By a dashed line in figure 4, we show the results obtained by solving (2) for a perfectly absorbing spherical boundary. The value of the Richardson constant, C_R, used to obtain the analytical result in figure 4, has been subject to some controversy [17]. We used here the most recent experimental value $C_R = 0.5$ supported also by numerical results [20], and find that this corresponds to $C = 0.32$. The flux curve found by the use of (2) differs in shape, and also in asymptotic value from the data obtained by the direct numerical simulation of the flow. We can make the asymptotic level to agree with the one obtained from the direct numerical simulation by choosing $C_R = 0.17$, approximately, which is, after all, not dramatically different from the generally accepted value. As far as the initial variation of the flux curve is concerned, it is obviously not possible to make the curve agree with the simulation results simply by changing C_R. The singularity around $t \approx 0$ for the calculated curve is due to the infinite density gradient at $t = 0$, see also figure 3. Such a singularity will be present in any model based on a diffusion equation, which takes a step-function as initial condition. It might be surprising that the solution of (2) gives an agreement which for the present problem is not as good as when the same equation is applied to studies of two-particle relative diffusion [17]. One reason may be that the latter problem only contains one length scale, namely the separation between the two particles. In the present case, the same length scale is used in the second-order structure function and then for constructing the effective diffusion coefficient. The equation is subsequently used for studying a problem containing a *different* length scale, namely the radius in the sphere of interception.

If we now consider the small radius limit, $\mathcal{R} \approx 0.2$, we find that our results are slowly deteriorating relative to the scaling (1). The relative uncertainty is increasing for these small separations, simply because there are relatively few particles being so close. There are several physical effects which become conspicuous for small separations: (1) intermittency, or (2) the influence of a viscous subrange, which are both properties of turbulent flows in general, and alternatively (3) the so-called "bottle-neck" effect, which is a feature of many numerical simulations of turbulent flows [22, 23]. Physically, the bottle-neck effect arises because of the finite resolution of the sub-Kolmogorov scales, giving a lack of small scale vortices, which makes the energy cascade less effective around the Kolmogorov scale, as compared to the ideal, physical, conditions. Some numerical results may indicate that the bottle-neck effect is a consequence of viscous effects stabilizing small vortex tubes against the kink instability [24]. The relative importance of these physical mechanisms is of course different for the two realizations listed in table 1. It might be added here that the bottle-neck effect is usually discussed in terms of the power spectra for the velocity fluctuation [23], but this is just a formality, since the structure function and power spectra are related by a simple Fourier transform. Also higher order correlations are interesting and can be obtained, see Appendix B, but these effects are not directly relevant for the present analysis.

The results corresponding to those shown in figure 4, but obtained for the second dataset are shown in figure 5. The empirical relation shown by the red curve is still from (6). This result, which was an excellent fit for the larger Reynolds number case, now falls approximately 2.5% above the present simulation results, but the general trend is still in good agreement. We note that the curve for the smallest radius, $\mathcal{R} = 0.2$, falls below the others. This is unambiguously attributed to the reduction in the second-order structure function, see figures 8 and 9, where

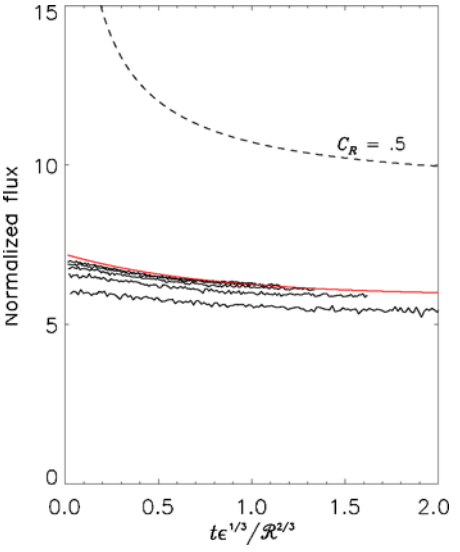

Figure 5. Normalized presentation of the data with $Re_\lambda = 183$, here for $\mathcal{R} \geq 0.2$ in steps of 0.1, up to 0.6. The dashed line represents result for the flux function obtained by solving (2). The red line gives the empirical relation (6).

the bending down is here assumed to be associated with the dissipation subrange. The smallest radius does not fully satisfy the restriction $\mathcal{R} \gg \eta \equiv (\nu^3/\epsilon)^{1/4}$.

To provide more details of the turbulent flow, we show in figure 6 the longitudinal and the total structure function $\langle (u_\parallel(0) - u_\parallel(r))^2 \rangle$ and $\langle (\mathbf{u}(0) - \mathbf{u}(r)) \cdot (\mathbf{u}(0) - \mathbf{u}(r)) \rangle$ for the reference case. The dashed lines are curves given by the Kolmogorov–Oubokhov result $C_K(\epsilon r)^{2/3}$, and $(11/3)C_K(\epsilon r)^{2/3}$, respectively. We used the analytical relation $\langle (u_\perp(0) - u_\perp(r))^2 \rangle = (4/3)\langle (u_\parallel(0) - u_\parallel(r))^2 \rangle$ between the longitudinal and transverse structure functions in the universal subrange, as derived from the Kolmogorov–Oubokhov relation. We show, in figure 7 also the corresponding compensated structure functions, obtained by division by $(\epsilon r)^{2/3}$. We find evidence for a universal subrange up to spatial separations of ~ 2 in the computational units. An interesting observation is that the plateau value corresponds to the Kolmogorov–Oubokhov constant, C_K, which is here determined as 2.10 ± 0.05. This value is in the accepted

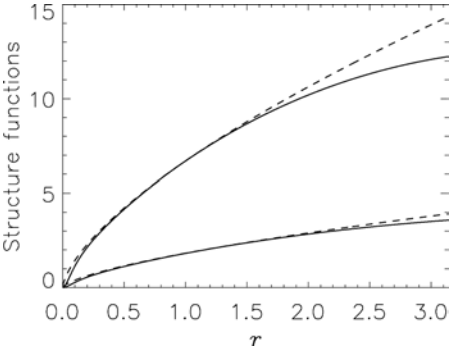

Figure 6. Numerically obtained structure functions. Dashed lines give a fit using $C_K(\epsilon r)^{2/3}$, with the Kolmogorov constant chosen as $C_K = 2.1$. The smallest separations are poorly resolved with the given number of particles.

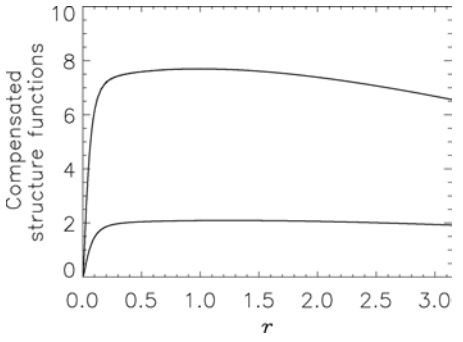

Figure 7. Compensated structure functions from figure 6.

range of 2–2.5 usually quoted [25, 26], but it is here determined with high accuracy. Note that the present analysis is carried out by analyzing particle trajectories, and not by analyzing the velocity field from the flow simulation as such. Since the particle positions are obtained by integration of the velocity field with a finite (but high) accuracy, the two results will not be perfectly identical.

For scales in the universal subrange but substantially larger than η in figure 7, we find an excellent agreement with the universal Kolmogorov–Oubokhov $(\epsilon r)^{2/3}$ scaling. With the given particle data, we are not able to resolve scales in the dissipative subrange: these scales are included in the simulation as such, see table 1, but the test particle spacing is on average too large to allow an acceptable signal-to-noise level in the estimator for these small scales.

We have obtained the structure functions also for the dataset with the smaller Reynolds number; see figures 8 and 9. In this case, we note that the best fit for the Kolmogorov–Oubokhov constant is here determined to be approximately $C_K = 2.05 \pm 0.05$, i.e. slightly below the previous value. Also the spatial interval for the validity of the ideal $(\epsilon r)^{2/3}$ scaling seems to be slightly reduced, implying that the universal subrange is not as well developed for the present case in comparison with the reference case. The reduced value for C_K is consistent with the observed reduction in turbulent particle flux in figure 5: since the turbulence level is slightly reduced as implied by the reduction in C_K, a reduction in turbulent flux is to be expected, as compared to the universal scaling.

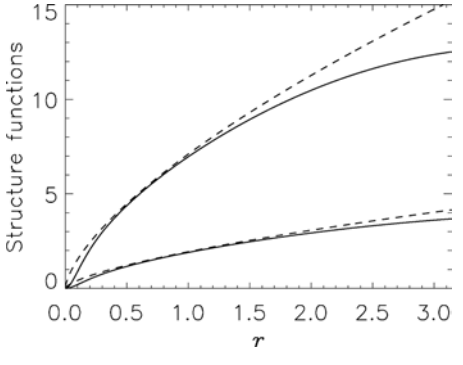

Figure 8. Numerically obtained structure functions for the case with $Re_\lambda = 183$. Dashed lines give a fit using $C_K(\epsilon r)^{2/3}$, with the Kolmogorov constant chosen as $C_K = 2.0$. The smallest separations are poorly resolved with the given number of particles.

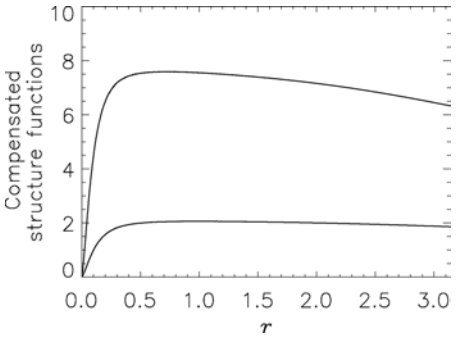

Figure 9. Compensated structure functions from figure Fig. 8. The slight tendency to a reduction in the compensated structure function for small separations is presumably the sign of a dissipation subrange.

5. Conclusions

In this correspondence, we have summarized the basic elements of a numerical method for investigating particle fluxes to a spherical surface moving with the flow. The problem has interest for the feeding process of aquatic micro-organisms. We found evidence for an accurate $\mathcal{R}^{7/3}$ flux scaling (see figure 4) in terms of the radius of a sphere of interception. In the asymptotic time limit, to the extent it can be reached in the present analysis, the data give a flux well approximated by (5), provided $\mathcal{R} < \mathcal{L}$, with $\mathcal{L}$ being the outer scale. The agreement in the asymptotic time limit can be made excellent by formally choosing a modified value for the Richardson constant. The present results agree well with similar results obtained by a laboratory experiment [16, 27], but here they are presented with a significantly improved signal-to-noise level. In particular, we are able to present an accurate comparison with results from a simple diffusion model, as in (2). The universal $\mathcal{R}^{7/3}\epsilon^{1/3}$-scaling resulting from (1) is confirmed for the universal range, where the Kolmogorov–Oubokhov law applies. We obtained an empirical result for the flux function F in (1), and in particular also its asymptotic constant value; see also figure 4. For very small radii in the reference spheres our results become uncertain, due to the relatively small number of close particles.

The results obtained for the reference dataset are, within 5%, consistent with results from a different simulation, with a somewhat reduced Reynolds number. The deviations can be explained by slight differences in the Kolmogorov–Oubokhov constant obtained from the two simulations. The results based on dimensional reasoning do not include intermittency effects, which do not seem to be important for the present phenomena. It might be that a significantly improved signal-to-noise ratio can reveal intermittency effects also for the present problem, but in that case we expect that noticeably larger Reynolds numbers should be used.

We emphasize that, as already mentioned, the present numerical results refer to a realization of the turbulence which is somewhat different from those in the experimental studies, where the ideas were tested first. We can thus argue that the results we obtained for the turbulent particle fluxes are robust. We note one important difference between numerical studies like the present one and the related laboratory experiments: here we use the average dissipated energy per. unit mass $\langle\epsilon\rangle$, which can be directly obtained. In laboratory experiments, this quantity is not so easily determined [8, 17, 18]. What is mostly used is the best fit of the Kolmogorov–Oubokhov law $C_K(\epsilon r)^{2/3}$. By using this procedure we ignore intermittency effects, i.e. the analysis does not distinguish $\langle\epsilon^{2/3}\rangle$ and $\langle\epsilon\rangle^{2/3}$, for instance.

With relevance for the biological aspect of the problem mentioned previously, we would like to point to one feature of the turbulent flux variation as illustrated in figure 2, which

allows us a qualitative discussion of self-induced motions of these small aquatic predators. Thus, the physical reason for the observed reduction in flux from $F(0)$ to $F(\infty)$ is that initially the predator is immersed in the maximal prey concentration. At later times this concentration is depleted in its near environment as seen from, for instance, figure 3. The asymptotic flux is determined by the balance of captured prey, and the transport of "fresh prey" into the search volume due to the turbulent mixing in the flow. An imagined "jump-pause" predator can move into a fresh fluid volume, which has not been searched for prey previously, by jumping a distance ℓ. Inspection of figure 3 indicates that $\ell/\mathcal{R} \sim 3$–4 suffices for this. In the "pause" phase, the predator is moving with the flow, and captures a prey-flux as the one illustrated in figure 2, starting at a value $n_0\epsilon^{1/3}\mathcal{R}^{7/3}F(0)$. The ratio $F(0)/F(\infty) \simeq 1.22$ (where the dimensional coefficient $\epsilon^{1/3}\mathcal{R}^{7/3}$ has canceled), is a measure for the maximum possible gain by this strategy. The precise numerical value for this gain is obtained most accurately by numerical simulations as the present ones.

The limit relevant for marine environments [8] will in general involve length scales of the same order, or larger, than the Kolmogorov scale. We suppose that the present observations justify extrapolation to radii, $\mathcal{R}$, in a universal subrange but smaller than those accessible here. It will be interesting to carry out an extension of the present study, where the dissipative subrange is better resolved, even if this will be on the expense of a fully developed universal subrange.

The problem discussed in the present study has relevance also for the analysis of coagulation of colloids in a turbulent environment [31]. As long as the geometrical size of the particles is much smaller than the Kolmogorov length scale, η, the classical analysis [32] is likely to apply. If, however, the size becomes larger than η, the rate of particle encounters will be dominated by turbulence effects as discussed here.

We found that the model diffusion equation (2) can serve only as an approximation, although it reproduces some overall features quite well. In order to obtain a general analytical model replacing a simple diffusion equation like (2), to give results for extended time periods and all $\mathcal{R}$, we will have to allow for a diffusion coefficient which depends on time as well as spatial separations, in particular including also memory effects [3].

Appendix A: Interpretations of the flux-depletion

The depletion of the flux to an absorbing spherical surface for increasing times as observed in, for instance, figure 4 and modeled by (6), has a simple physical interpretation: at the time of release, the spherical surface is surrounded by a statistically uniform distribution of point particles at maximum concentration n_0. For increasing times, some of these particles are absorbed and there is a non-vanishing probability for the sphere to enter, at least partially, a region of the fluid which has already been evacuated. We can imagine the sphere to be trailed by a cylindrical region with radius $\mathcal{R}$, with this region being deformed by the turbulent motions in the flow. The volume of the "evacuated" fluid increases slower than linearly with time, since there is, as said, a finite probability to pass through such regions several times. Using (6), we can evidently interpret the ratio $P_\infty \equiv 1 - F(\infty)/F(0) \approx 0.18$ as the asymptotic probability for a surface element of the reference sphere to enter a region which is void of marker particles. By asymptotic we here mean $t \gg \tau_0 \equiv 0.77\ \mathcal{R}^{2/3}/\epsilon^{1/3}$, where τ_0 is the time constant in (6). It is important to note that P_∞ is, at least formally, independent of $\mathcal{R}$ as well as ϵ, the implied restriction being that $\mathcal{R} > \eta \equiv (\nu^3/\epsilon)^{1/4}$ for the scale size of the sphere being in the universal subrange, with η being the Kolmogorov scale expressed in terms of ϵ and the kinematic viscosity ν. Since η can be very small for realistic flow conditions,

we can use P_∞ as an estimate also for infinitesimal spherical scales. Since $F(\infty) > 0$ for three-dimensional incompressible turbulence, there is a finite probability that parts of the fluid are never traversed by the reference sphere, irrespective of its size, as long as the turbulence volume can be considered infinite.

It can be instructive to compare the foregoing results for what is obtained by simple diffusive Brownian motion for spherically symmetric conditions. In this case, the flux to the surface is obtained as $J(t) = -4\pi D\mathcal{R}^2 \partial n(r, t)/\partial r|_{r=\mathcal{R}}$, where the space-time variation of the marked particle density is determined by the diffusion equation $\partial(rn)/\partial t = D\partial^2(rn)/\partial r^2$, here written for spherical symmetry, with D being the constant diffusion coefficient. We find

$$J(t)/n_0 = 4\pi D\mathcal{R}\left(1 + \frac{\mathcal{R}}{\sqrt{\pi Dt}}\right). \tag{A1}$$

The analysis can be found in the literature [32, 33]. Evidently, $J(0)$ diverges due to the form of the diffusive flux which contains a gradient, which is infinite for $t = 0$ for the present conditions, and we cannot here define the ratio $J(\infty)/J(0)$. On the other hand, we still have $J(\infty) > 0$, and can argue also here for a finite probability at $t \to \infty$ for fluid elements not being visited.

The analysis outlined before refers to an absorbing surface at rest. In case the sphere is itself participating in a diffusive motion, the relative motion of the particles involved should be considered [32]. This can, for the present simple case, be done by replacing the diffusion constant D in (A1) with $2D$.

The result (A1) applies for diffusion in three spatial dimensions. If we repeat the analysis for diffusion in *two* dimensions, we find after some algebra the normalized diffusive flux through a cylinder segment of interception of length $\mathcal{L}$ to be

$$J(t)/n_0 = \mathcal{L}\mathcal{R}D\frac{8}{\pi}\int_0^\infty \frac{\mathrm{e}^{-\lambda^2 Dt}}{J_0^2(\lambda\mathcal{R}) + Y_0^2(\lambda\mathcal{R})}\frac{\mathrm{d}\lambda}{\lambda}, \tag{A2}$$

in terms of Bessel functions J_0 and Y_0. (The analysis turns out to be slightly more complicated than the three-dimensional case [16].) Evidently, the flux does not reach a stationary level for $t \to \infty$ in this case, $J(t \to \infty) \to 0$. For two dimensions all of the fluid will be traversed as $t \to \infty$. This observation is consistent with the properties of a random walk model [34], where a diffusion equation models a limiting case.

From a general diffusion model like $\partial n/\partial t = \nabla\cdot D(\mathbf{r}, t)\nabla n$ we readily obtain a diffusion flux density in the form $\mathbf{f}(\mathbf{r}, t) = -D(\mathbf{r}, t)\nabla n$. The expression (2) is a special case of this general diffusion equation. A diffusion *velocity* is then found as $\mathbf{U} \equiv \mathbf{f}/n = -D(\mathbf{r}, t)\nabla \ln n$, where we for the most general case allow for both a space and time dependence of the diffusion coefficient D. For the special case (2), we have the diffusion coefficient being a function of position only. The important observation is now that the diffusion velocity is in general *compressible*, $\nabla \cdot \mathbf{U} \neq 0$, and it therefore does not properly represent the underlying velocity field for the present problem. Any model based on a diffusion equation like the one mentioned before will have this property. The only way to "patch-up" the diffusion velocity will be to let D depend on density, which seems unacceptable here.

Appendix B: Triple velocity correlations

Although not directly relevant for the present analysis, we found it worthwhile to study also third-order correlation functions, in particular $U^3k(r) \equiv \langle u_\parallel^2(0)u_\parallel(r)\rangle$; see figure 10. We

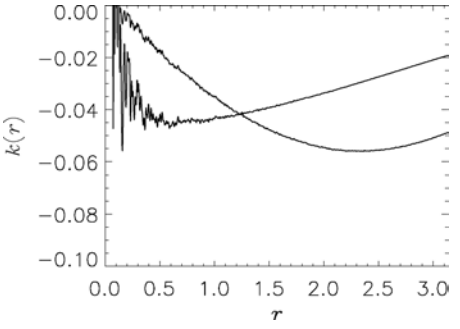

Figure 10. The triple correlation function $k(r) \equiv \langle u_\parallel^2(0)u_\parallel(r)\rangle / U^3$. Note that the magnitudes of the normalized triple correlations are smaller than for second-order structure functions, so the noise level is more apparent. We have here $Re_\lambda = 286$. Also the compensated function $k(r)/(\epsilon r)$ is shown.

introduced $U^2 \equiv \frac{1}{3}\langle u^2\rangle$. Other triple correlations can be derived from $k(r)$, given homogeneous and isotropic conditions [35]. Also here we attempt a compensated presentation, here carried out by division by (ϵr), which is the simplest extension of the Kolmogorov dimensional arguments. We find that a plateau is not evident here, in contrast to the case of the compensated second-order structure functions. We can nonetheless determine a constant C_k in an approximation for small r, with $U^3 k(r) \approx C_k \epsilon r$. We find $C_k \approx -0.05$, which is in fair agreement with experimental results [36]. It is not probable to find particles with very small separations with the available data, and this gives enhanced uncertainties for small separations. For the dataset with $Re_\lambda = 183$, the number of particles is even smaller than for the reference set, and the noise level correspondingly larger. For these other data we find the same features as shown in figure 10, see figure 11, but the signal-to-noise ratio is slightly worse. Seemingly, the numerical coefficient in $k(r)$ decreases slightly with decreasing Reynolds number, but at present we only have these two datasets, and the trend cannot be further quantified.

The result $\langle (u_\parallel(0) - u_\parallel(r))^3\rangle = -\frac{4}{5}\epsilon r$ is supposed to be exact [37] for infinite Reynolds numbers. With this result and $\langle u_\parallel^2(0)u_\parallel(r)\rangle = -\langle u_\parallel^2(0)u_\parallel(-r)\rangle$, we find in the large Reynolds number limit $C_k^{(\infty)} = -4/30 \approx -0.13$, i.e. approximately twice the number we found before. It is, however, obvious that the present Reynolds number, see table 1, is not sufficiently large to allow the use of the limiting value of C_k for $Re_\lambda \to \infty$.

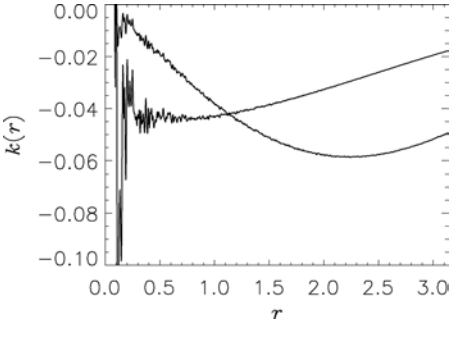

Figure 11. The triple correlation function $k(r) \equiv \langle u_\parallel^2(0)u_\parallel(r)\rangle / U^3$ for the smaller dataset. We have here $Re_\lambda = 183$. The compensated function $k(r)/(\epsilon r)$ is shown here as well.

Acknowledgements

Two of the authors (HLP and JT) were in part supported by the ECOBE project, Norwegian National Science Foundation under contract NFR-136030/431. The authors acknowledge the hospitality of the Norwegian Centre for Advanced Studies, under the project "Turbulence in Fluids and Plasmas". We thank Jakob Mann and Søren Ott for valuable discussions.

References

[1] Richardson, L.F., 1926, Atmospheric diffusion shown as a distance-neighbour graph. *Proceedings of the Royal Society of London, Series A*, **6**, 709–737.
[2] Batchelor, G.K., 1952, Diffusion in a field of homogeneous turbulence II. The relative motion of particles. *Proceedings of the Cambridge Philosophical Society (London)*, **48**, 345–362.
[3] Roberts, P.H., 1961, Analytical theory of turbulent diffusion. *Journal of Fluid Mechanics*, **11**, 257–283.
[4] Muelbert, J.H., Lewis, M.R. and Kelley, D.E., 1994, The importance of small-scale turbulence in the feeding of herring larvae. *Journal of Plankton Research*, **16**, 927–944.
[5] Rothschild, B.J. and Osborn, T.R., 1988, Small-scale turbulence and plankton contact rates. *Journal of Plankton Research*, **10**, 465–474.
[6] Kiørboe, T. and Saiz, E., 1995, Planktivorous feeding in calm and turbulent environments, with emphasis on copepods. *Marine Ecology Progress Seriers*, **122**, 135–145.
[7] Osborn, T., 1996., The role of turbulent diffusion for copepods with feeding currents. *Journal Plankton Research*, **18**, 185–195.
[8] Hill, P.S., Nowell, A.R.M. and Jumars, P.A., 1992, Encounter rate by turbulent shear of particles similar in diameter to the Kolmogorov scale. *Journal of Marine Research*, **50**, 643–668.
[9] Yamazaki, H., Osborn, T.R. and Squires, K.D., 1991, Direct numerical simulation of planktonic contact in turbulent flow. *Journal of Plankton Research*, **13**, 629–643.
[10] Biferale, L., Boffetta, G., Celani, A., Lanotte, A. and Toschi, F., 2005, Particle trapping in three-dimensional fully developed turbulence. *Physics of Fluids*, **17**, 021701.
[11] Granata, T.C. and Dickey, T.D., 1919, The fluid mechanics of copepod feeding in turbulent flow: a theoretical approach. *Progress in Oceanography*, **26**, 243–261.
[12] Blaxter, J.H.S. and Staines, M.E., 1971, Food searching potential in marine fish larvae. In D.J., Crisp (ed), *Proceedings of the 4th European Marine Biology Symposium* (Cambridge University Press, UK), pp. 467–485. Cambridge University Press, UK.
[13] Lewis, D.M. and Pedley, T.J., 2000, Planktonic contact rates in homogeneous isotropic turbulence: theoretical predictions and kinematic simulations. *Journal of Theoretical Biology*, **205**, 377–408.
[14] Tennekes, H. and Lumley, J.L., 1972, *A First Course in Turbulence*, (Cambridge, MA: The MIT press).
[15] Morse, P.M. and Feshbach, H., 1953, *Methods of Ttheoretical Pphysics*. International series in pure and applied physics. (New York: McGraw-Hill, New York).
[16] Mann, J., Ott, S., Pécseli, H.L. and Trulsen, J., 2005, Turbulent particle flux to a perfectly absorbing surface. *Journal of Fluid Mechanics*, **534**, 1–21.
[17] Ott, S. and Mann, J., 2000, An experimental investigation of the relative diffusion of particle pairs in three dimensional turbulent flow. *Journal of Fluid Mechanics*, **422**, 207–223.
[18] Mann, J., Ott, S. and Andersen, J.S., 1999, Experimental study of relative, turbulent diffusion. Technical Report Risø-R-1036(EN), Risø National Laboratory, DK-4000 Roskilde, Denmark, 1999. Can be downloaded from http://www.risoe.dk/rispubl/VEA/ris-r-1036.htm.
[19] Lesieur, M., 1997, *Turbulence in Fluids*. (Kluwer, Dordrecht: Kluwer), 3rd edition.
[20] Boffetta, G. and Sokolov, I.M., 2002, Relative dispersion in fully developed turbulence: the Richardson law and intermittency corrections. *Physical Review Letters*, **88**, 094501.
[21] Virant, M. and Dracos, T., 1997, 3D PTV and its application on Lagrangian motion. *Measurement Science and Technology*, **8**, 1529–1552.
[22] Lohse, D. and Müller-Groeling, A., 1996, Anisotropy and scaling corrections in turbulence. *Physical Review E*, **54**, 395–405.
[23] Dobler, W., Haugen, N.E.L., Yousef, T.A. and Brandenburg, A., 2003, Bottleneck effect in three-dimensional turbulence simulations. *Physical Review E*, **68**, 026304.
[24] Woodward, P.R., Porter, D.H., Edgar, B.K., Anderson, S. and Bassett, G., 1995, Parallel computation of turbulent fluid-flow. *Computational and Applied Mathematics*, **14**, 97–105.
[25] Hinze, J.O., 1975, *Turbulence*. (New York: McGraw-Hill), New York, 2nd edition, 1975.
[26] Monin, A.S. and Yaglom, A.M., 1975, *Statistical Fluid Mechanics*, vol. 2. (The Cambridge, MA: MIT press), Cambridge, Massachusetts.
[27] Mann, J., Ott, S., Pécseli, H.L. and Trulsen, J., 2002, Predator-prey encounters in turbulent waters. *Physical Review E*, **65** 026304.
[28] MacKenzie, B.R., Miller, T.J., Cyr, S. and Leggett, W.C., 1994, Evidence for a dome-shaped relationship between turbulence and larval fish ingestion rates. *Limnologia Oceanography*, **39**, 1790–1799.

[29] Mann, J., Ott, S., Pécseli, H.L. and Trulsen, J., 2003, Experimental studies of occupation times in turbulent flows. *Physical Review E*, **67**, 056307.
[30] Berg Jørgensen, J., Mann, J., Ott, S., Pécseli, H.L. and Trulsen, J., 2005, Experimental studies of occupation and transit times in turbulent flows. *Physics of Fluids*, **17**, 035111.
[31] Delichatsios, M.A. and Probstein, R.F., 1975, Coagulation in turbulent flow—theory and experiment. *Journal of Colloid Interface Science*, **51**, 394–405.
[32] Chandrasekhar, S., 1954, Stochastic problems in physics and astronomy. In N. Wax (ed), *Selected Papers on Noise and Stochastic Processes* (New York: Dover) pp. 3–91. Dover, New York.
[33] Pécseli, H.L., 2000, *Fluctuations in Physical Systems* (Cambridge: Cambridge University Press), Cambridge, UK.
[34] Cox, D.R. and Miller, H.D., 1965, *The Theory of Stochastic Processes* (London: Chapman & Hall), London.
[35] Batchelor, G.K., 1953. *The Theory of Homogeneous Turbulence* (Cambridge, Cambridge University Press).
[36] Van Atta, C.W. and Chen, W.Y., 1968, Correlation measurements in grid turbulence using digital harmonic analysis. *Journal of Fluid Mechanics*, **34**, 497–515.
[37] Van Atta, C.W. and Chen, W.Y., 1970, Structure functions of turbulence in the atmospheric boundary layer over the ocean. *Journal of Fluid Mechanics*, **44**, 145–159.